Novel cobalt-free CO2-tolerant dual-phase membranes of Ce0.8Sm0.2O2−δ –Ba0.95La0.05Fe1−xZrxO3−δ for oxygen separation

Cheng, Hongwei; Luo, Longfei; Yao, Weilin; Lu, Xionggang; Zou, Xingli; Zhou, Zhongfu

Published in:
Journal of Membrane Science

DOI:
10.1016/j.memsci.2015.05.057

Publication date:
2015

Citation for published version (APA):
Cheng, H., Luo, L., Yao, W., Lu, X., Zou, X., & Zhou, Z. (2015). Novel cobalt-free CO2-tolerant dual-phase membranes of Ce0.8Sm0.2O2−δ –Ba0.95La0.05Fe1−xZrxO3−δ for oxygen separation. *Journal of Membrane Science*, *492*, 220-229. https://doi.org/10.1016/j.memsci.2015.05.057

www.elsevier.com/locate/memsci

Novel cobalt-free CO_2-tolerant dual-phase membranes of $Ce_{0.8}Sm_{0.2}O_{2-\delta}$ – $Ba_{0.95}La_{0.05}Fe_{1-x}Zr_xO_{3-\delta}$ for oxygen separation

Hongwei Cheng, Longfei Luo, Weilin Yao, Xionggang Lu, Xingli Zou, Zhongfu Zhou

PII: S0376-7388(15)00495-0
DOI: http://dx.doi.org/10.1016/j.memsci.2015.05.057
Reference: MEMSCI13739

To appear in: *Journal of Membrane Science*

Received date: 5 February 2015
Revised date: 6 May 2015
Accepted date: 25 May 2015

Cite this article as: Hongwei Cheng, Longfei Luo, Weilin Yao, Xionggang Lu, Xingli Zou, Zhongfu Zhou, Novel cobalt-free CO_2-tolerant dual-phase membranes of $Ce_{0.8}Sm_{0.2}O_{2-\delta}$ –$Ba_{0.95}La_{0.05}Fe_{1-x}Zr_xO_{3-\delta}$ for oxygen separation, *Journal of Membrane Science,* http://dx.doi.org/10.1016/j.memsci.2015.05.057

Novel cobalt-free CO_2-tolerant dual-phase membranes of $Ce_{0.8}Sm_{0.2}O_{2-\delta}$–$Ba_{0.95}La_{0.05}Fe_{1-x}Zr_xO_{3-\delta}$ for oxygen separation

Hongwei Cheng [a,b]*, Longfei Luo [a], Weilin Yao [a], Xionggang Lu [a,b*], Xingli Zou [a,b], Zhongfu Zhou [a,b,c]

[a] *School of Materials Science and Engineering, Shanghai University, Shanghai 200072, People s Republic of China*

[b] *State Key Laboratory of Advanced Special Steel, Shanghai University, Shanghai 200072, People s Republic of China*

[c] *Institute of Mathematics and Physics, Aberystwyth University, Aberystwyth SY23 3BZ, United Kingdom*

Abstract: A novel series of cobalt-free dense oxygen-permeable dual-phase membranes with a composition of 60 wt% $Ce_{0.8}Sm_{0.2}O_{2-\delta}$–40 wt% $Ba_{0.95}La_{0.05}Fe_{1-x}Zr_xO_{3-\delta}$ (SDC–BLFZ, x = 0–0.20) are successfully developed and systematically evaluated as potential oxygen transport membranes for oxy-fuel combustion. The effects of substituting zirconium for iron on the structural characteristics, oxygen permeability, and CO_2 resistance of these membranes are studied. Experimental results show that appropriate doping of zirconium slightly decreases the oxygen permeability of the SDC–BLFZ membranes under helium but significantly enhances the structural stability and CO_2 tolerance. For the sample with x = 0.15, a stable oxygen permeation flux of 0.24 ml min^{-1} cm^{-2} was achieved at 925 °C for a 1.0 mm thick membrane with CO_2 as the sweep gas for more than 80 h. This flux value is only 19% lower than that under an air/He gradient, which is much better than that obtained with most alkaline-metal-containing composite dual-phase membranes. The enhanced CO_2 tolerance of the Zr-doped SDC–BLFZ membranes is

* Corresponding author. Tel./Fax: +86-21-56335768.
E-mail: hwcheng@shu.edu.cn (H.W. Cheng); luxg@shu.edu.cn (X.G. Lu).

attributed to the declining basicity of BLFZ induced by the substitution of Fe by Zr, as revealed by X-ray photoelectron spectroscopy (XPS). The stable oxygen permeability of the SDC–BLFZ membranes under CO_2 demonstrates the potential application of SDC–BLFZ in oxy-fuel combustion technology.

Keywords: oxygen permeation; dual-phase membrane; CO_2 tolerance; basicity; zirconium

1. Introduction

The capture and storage of carbon has been proposed to reduce the escalating levels of atmospheric carbon dioxide emissions, as CO_2 is believed to be mainly responsible for global warming [1,2]. Oxy-fuel combustion, in which oxygen is used instead of air for the combustion of fossil fuels, is considered as a promising technology for CO_2 sequestration [3,4]. Unfortunately, the high cost of pure oxygen and other problems have prevented its popularity. Since oxygen separated by oxygen transport membranes (OTMs) can be significantly cheaper than that separated by pressure swing adsorption technology, a new concept of oxy-fuel combustion, i.e., oxy-fuel combustion integrated with OTMs, has attracted increasing interest [5,6]. Since one side of the OTMs is exposed to the products, which contain large amounts of CO_2, the OTMs applied to oxygen combustion must exhibit not only good oxygen permeation but also favorable CO_2 resistance [7].

Since the pioneering study of Teraoka *et al.* [8] in 1985 on $La_{1-x}Sr_xCo_{1-y}Fe_yO_3$, an increasing number of studies have been focused on perovskite (formula: ABO_3) mixed ionic-electronic conductivity (MIEC) composites because of their impressive oxygen permeability [9]. In most of these composites, a part or even all of the A-site lattices are occupied by alkaline-earth metal ions. Despite their impressive oxygen permeability under inert atmospheres, many researchers have observed that

alkaline-earth-metal-containing membranes easily react with CO_2 and form carbonates on the surface, resulting in the degradation or even failure of oxygen permeation [10,11]. Some progress has been made in enhancing the CO_2 tolerance of perovskite composites, e.g., by the reduction or elimination of alkaline-earth metals in the A-site [12,13] and doping of the B-site with an appropriate amount of stable metals such as niobium or tantalum [14,15]. Another way to enhance their CO_2 tolerance is to introduce secondary CO_2-stable ionic-conducting (IC) phase such as $Ce_{0.8}Gd_{0.2}O_{2-\delta}$ (CGO) to construct dual-phase membranes. For example, an instant cease of oxygen permeation was observed for the state-of-the-art $Ba_{0.5}Sr_{0.5}Co_{0.8}Fe_{0.2}O_{3-\delta}$ (BSCF) exposed to CO_2, whereas a part of the permeation flux was retained for the CGO–BSCF [16,17]. In such dual-phase membranes, the perovskite phase serves as the electronic-conducting (EC) phase, where electrons are transported through the EC phase, and oxygen ions are transported through both the EC and IC phase. Since the IC phase shows high chemical stability against CO_2 and will not react with it, the membrane surface will not be completely covered by carbonates, and oxygen permeation can be partly reserved.

Thus far, cobalt-based perovskite composites are one of the most popular materials in the family of MIEC composites. Generally, cobalt-containing perovskite membranes exhibit outstanding oxygen permeability. However, cobalt-based oxides pose several disadvantages such as the high cost of cobalt and relatively larger linear expansion coefficients, which will lead to instability in the structure of the membranes, as well as the introduction of microcracks, under reducing atmosphere [18,19]. Besides, cobalt-containing membranes are less stable in CO_2 than that of iron-base composites, which makes them less suitable for oxy-fuel combustion [10]. Efforts have been made to develop cobalt-free perovskite composites, among which

iron-based oxides are unique because of their preferable oxygen permeability and relatively better stability under operating conditions [20]. Recently, partially A-site La-doped $BaFeO_{3-\delta}$-based composites of $Ba_{0.95}La_{0.05}FeO_{3-\delta}$ have aroused intense interest as OTMs and cathode materials for solid oxide fuel cells [21,22].

In this paper, a series of 60 wt% $Ce_{0.8}Sm_{0.2}O_{2-\delta}$–40 wt% $Ba_{0.95}La_{0.05}Fe_{1-x}Zr_xO_{3-\delta}$ (SDC–BLFZ) dual-phase OTMs with SDC as the IC phase and BLFZ as the EC phase were successfully fabricated. Herein, we added the secondary SDC phase to BLFZ to take advantage of its excellent CO_2 resistance. The effects of zirconium substitution on the structure stability of BLFZ under different atmospheres, chemical compatibility between the two phases, oxygen permeability, and chemical stability of SDC–BLFZ against CO_2 were systemically studied.

2. Experimental

2.1. Synthesis of powders and membranes

The SDC precursor was synthesized by a combined EDTA–citrate complexing sol–gel method as mentioned in our earlier study [23]. Briefly, a stoichiometric amount of Sm_2O_3 and $Ce(NO_3)_2{\cdot}6H_2O$ was added to a beaker with distilled water, and excess concentrated nitric acid was added to dissolve Sm_2O_3. Calculated molar citric acid and EDTA at a ratio of citric acid: EDTA: metal nitrates = 1.5:1:1 were added to the mixed solution, and an appropriate amount of $NH_3{\cdot}H_2O$ was introduced till the solution pH reached ca. 6 and the solution was clear and transparent. The sol was heated at 80 °C using a rotary evaporator till most of the water was evaporated. The resultant gel was fired at 350 °C in air to remove the organic compounds. The resultant powder was carefully ground and calcined at 600 °C for 5 h. BLFZ powders were fabricated by a similar route except that the calcination temperature was 850 °C.

The resultant SDC and BLFZ powders were weighed in a ratio of 60:40 and

carefully ground for 4 h in a mortar to ensure the uniformity of the two powders. The mixed powders were pressed to disks by a uniaxial dry-pressing process and then sintered at 1200 °C for 5 h in static air.

2.2. Material characterization

The phase structure of the as-prepared powders and membranes as well as the spent membranes was investigated by X-ray diffraction (XRD, Rigaku D/MAX2550 powder diffractometer, Cu Kα radiation, λ = 1.54056 Å) in an angle range between 20° and 90° with 0.02° intervals. The oxygen desorption property of the BLFZ powders was tested by oxygen temperature-programmed desorption (O_2-TPD) experiments using Micrometrics AutoChem II 2920. Samples of approximately 500 mg were placed in a fixed-bed U-shaped quartz reactor. They were first heated at 120 °C for 10 min under He and then cooled to room temperature, followed by heating to 1000 °C at a constant rate of 10 °C min^{-1} in flowing He (30 ml min^{-1}). Thermogravimetry and differential scanning calorimetry (TG-DSC) measurements were performed to study the CO_2 resistance of SDC–BLFZ membranes using a NETZSCH STA 449F3. The membranes were ground into fine powders and heated from 100 °C to 1150 °C in a gas mixture containing 50 vol% CO_2 and N_2 at a heating rate of 10 °C min^{-1}. Isothermal gravimetric analysis was also performed at 950 °C in the same atmosphere. The O 1s binding energy and oxidation state of Fe ions in BLFZ were measured by X-ray photoelectron spectroscopy (XPS, ESCALAB 250Xi) with Al Kα radiation and analyzed using XPSPeak 4.1. Before analysis, the XPS data were normalized using the binding energy value of adventitious carbon at 284.6 eV as reference. The surface morphology of the fresh sintered and spent membranes was examined by scanning electron microscopy (SEM, Hitachi SU70).

2.3. Oxygen permeability measurement

The oxygen permeability of through SDC–BLFZ membranes was measured by an online gas chromatography (GC–9160) system connected to a home-made high-temperature cell [24]. The membranes were polished to a desired thickness using abrasive paper and then sealed onto a quartz tube with a silver ring softened at melting point. Effective sealing was ensured before the oxygen permeability measurements to avoid the leakage of any oxygen that could contribute to the permeation flux. The feed side of the membrane was exposed to flowing ambient air at a flow rate of 300 ml min^{-1}, and the sweep side was swept by He, CO_2, or a gas mixture of He and CO_2 at a flow rate of 100 ml min^{-1}. The oxygen permeation fluxes through the membranes were calculated from the oxygen content in the permeated gas detected by gas chromatography according to the equation reported by Li [25].

3. Results and discussion

3.1. Structure and stability

Fig. 1(a) shows the XRD patterns of the SDC and BLFZ powders calcined at 650 and 850 °C for 5 h in air, respectively. As shown in the figure, the SDC pattern is well indexed to $Ce_{0.8}Sm_{0.2}O_{2-\delta}$ (JCPDS # 75-0158) with a fluorite structure [26]. The calculated average lattice constant of SDC is 5.44 Å. For BLF without any Zr substitution, all reflection peaks are perfectly indexed to a cubic perovskite structure, and no impurity phases are detected. Its average lattice constant is calculated to be 4.00 Å, which is consistent with the results reported by Kida and Dong [21,27]. For BLFZ powders, the peaks assigned to the (110) plane shift toward lower angles with increasing Zr content, indicative of the expansion of lattice parameters induced by the larger Zr radius. In addition, characteristic peaks assignable to ZrO_2 are observed for samples with x = 0.15 and 0.20, demonstrating that the solid solubility of Zr in BLF is lower than 0.15. A similar phenomenon has been observed for doped $SrCoO_{3-\delta}$ [18].

Because the standard XRD patterns of BLFZ are not available, it's difficult to figure out the exact composition of BLFZ and the content of ZrO_2. However, for the sake of simplicity, we still describe the composition as BLFZ according to its nominal chemical composition herein.

Fig. 1(b) shows the XRD patterns of SDC–BLFZ membranes sintered at 1200 °C for 5 h. For dual-phase composites, it is well known that the reaction between the two phases and the resulting foreign phases could have negative effects on their performance. Fortunately, for SDC–BLF, all reflection peaks are perfectly assigned to SDC and BLF with no obvious foreign phases generated by the reaction of the two phases, suggesting good chemical compatibility between SDC and BLF. As the Zr content increases, the reflection peaks assignable to BLFZ become shorter and wider, indicating that the excess oversized Zr ions induces a worse-developed crystallization and lattice distortion of BLFZ. For the sample with x = 0.20, peaks of $BaZrO_3$ are clearly observed, and ZrO_2 detected for the samples with x = 0.15 and 0.20 in the calcined BLFZ powders disappears. Since the sintering temperature of SDC-BLFZ membranes is much higher than that of BLFZ powders, the residual ZrO_2 has possibly reacted with barium oxide and formed $BaZrO_3$ during sintering at 1200 °C [28,29]. Since $BaZrO_3$ is non-conducting to oxygen ions, it is not advisable to substitute too much of Zr for Fe.

The structure stability of BLFZ under low oxygen partial pressure was investigated by O_2-TPD, as shown in Fig. 2. All samples exhibit a similar oxygen desorption peak at approximately 485 °C, which shifts slightly to high temperatures with increasing Zr content. Besides, the onset desorption temperature is increased, and the peak areas become smaller as the Zr content increases. These results indicate that the average metal–oxygen binding energy increases with increasing zirconium content

[30]. The oxygen desorption peak at intermediate temperatures and elevated temperatures is assigned to α-O_2 desorption and β-O_2 desorption, which are attributed to the reduction of Fe^{4+} to Fe^{3+} and Fe^{3+} to Fe^{2+}, respectively [29]. Thus, it is reasonable to speculate that the oxidation of Fe^{3+} to the higher-valence Fe^{4+} is suppressed by the substitution of Zr for Fe [9]. A β-O_2 desorption peak is detected at 899 °C for BLF. Since the reduction of Co^{3+} to Co^{2+} has been repeatedly reported to be responsible for the instability of many cobalt-based composites, it can be reasonably concluded that the structure stability of BLFZ under low oxygen partial pressure is enhanced by the partial substitution of Zr for Fe, albeit at the expense of a smaller amount of desorbed oxygen.

3.2. XPS analysis

To verify the abovementioned assumption that the oxidation of Fe^{3+} to Fe^{4+} is suppressed by doping with Zr, XPS is performed to determine the oxidation state of Fe ions in BLFZ. Before analysis, all raw XPS data are normalized by using the C 1s peak of adventitious carbon at 284.6 eV as reference [31]. As shown in Fig. 3, two peaks assigned to Fe $2p_{1/2}$ and Fe $2p_{3/2}$ are observed at 709.68/723.38 and 709.78/723.28 eV for samples with x = 0 and x = 0.10, respectively, and a satellite peak at 718.28 eV is detected for both samples. The peaks were subsequently de-convoluted into two peaks by employing two valence states of Fe, i.e., Fe^{4+} and Fe^{3+}, respectively [32]. The Shirley background was subtracted, and the peak area of Fe $2p_{3/2}$ was set to two times that of Fe $2p_{1/2}$ in the curve fitting [33]. By the curve fitting of the two peaks, the Fe^{4+} and Fe^{3+} concentrations are calculated, as listed in Fig. 3. The Fe^{4+} concentration decreases from 61% to 51% as the doping amount of Zr increases from 0 to 0.10, which is in accordance with charge compensation and O_2-TPD experimental results shown in Fig. 2. This result is also in agreement with

$La_{0.3}Sr_{0.7}Ti_{1-x}Co_xO_3$ oxides, in which the Co^{4+} concentration decreases from 48% to 24% with an increase in the Ti content from 0.40 to 0.55 [34]. A chemical shift to a higher binding energy was observed for the doublet peaks assigned to both Fe^{4+} and Fe^{3+}, which can be attributed to the stronger Zr–O bond energy as compared to that of Fe–O.

Since XPS technology is employed to gain insight into the O 1s binding energy, which is an important parameter that significantly affects the reaction between metal oxides and CO_2, it is also employed to study the effect of Zr content on the CO_2 resistance of BLFZ [5,35]. According to the Lewis acid–base theory, the basicity of metal oxides can be defined as their ability to donate electrons. The higher O 1s binding energy suggests that it is more difficult for the metal oxides to donate electrons [36]. By employing three different binding energy values, the raw XPS spectra of O 1s are de-convoluted into three peaks, which can be assigned to lattice oxygen, absorbed oxygen, and absorbed water, respectively [15,35]. As listed in Fig. 4, the O 1s binding energy corresponding to lattice oxygen increases with increasing amounts of doped Zr, from 527.94 eV (x = 0) to 528.25 eV (x = 0.10). Evidently, Zr doping successfully lowers the basicity of BLF.

3.3 Thermogravimetric analysis

To evaluate the influence of Zr doping on the CO_2 tolerance of SDC–BLFZ, TG-DSC experiments were conducted using a gas mixture of 50 vol% CO_2 and N_2 from 100 °C to 1150 °C, as shown in Fig. 5(a). All samples experience a distinct weight loss in the initial stage of the experiment below 300 °C, probably originating from the desorption of the absorbed gas mixture on the powder samples and the evaporation of water [34]. A distinct mass gain is observed for the sample with x = 0, and a small one is detected for that with x = 0.05, which originates from the formation

of carbonates generated by the reaction between Ba^{2+} and CO_2 [23,37]. In addition, a rapid weight loss is observed for the former at ca. 1050 °C, and a corresponding endothermic peak is detected in the DSC curves, which is ascribed to the decomposition of the resultant carbonates. As demonstrated by O_2-TPD, the lattice oxygen of BLFZ starts to desorb at 350 °C; hence, the weight gain above this temperature is a combined effect of the weight gain originating from the formation of carbonates and the weight loss stemming from the desorption of lattice oxygen [38,39]. Since no weight increase is observed for samples with x = 0.10–0.20, it is reasonable to assume that the reaction between SDC–BLFZ and CO_2 is significantly or even totally restrained. Obviously, Zr doping successfully enhances the CO_2 resistance of SDC–BLFZ, probably caused by a weaker basicity induced by the stronger binding energy of Zr–O as compared to that of Fe–O, as illustrated by the O 1s binding energy in the XPS experiments.

Isothermal gravimetric analysis was also performed on the samples with x = 0 and x = 0.15 to gain insight into the relationship between Zr substitution and CO_2 resistance. The two samples were also treated in a gas mixture of 50 vol% CO_2 and N_2 with increasing temperatures from 100 °C to 950 °C at a rate of 10 °C min^{-1} and then maintained at 950 °C for 3 h, as shown in Fig. 5(b). Similar to that observed in Fig. 5(a), a distinct weight loss was also observed at the initial stage of the experiment. Above 465 °C, a maximum mass gain of 0.86% was observed for the sample with x = 0, whereas a continuous weight decrease reaching 0.51% was detected for that with x = 0.15. The result indicates that Zr doping significantly enhances the CO_2 resistance of SDC–BLFZ. Notably, the maximum mass gain of 0.86% is rather smaller in comparison to that observed for many single-phase perovskite composites [5,14,15,35], probably because of the protection provided by fluorite SDC to

perovskite BLF.

3.4. Oxygen permeability and CO_2 tolerance

Fig. 6(a) shows the temperature dependence of oxygen permeation flux through 1 mm thick SDC–BLFZ membranes using He as the sweep gas. From the figure, the oxygen permeation flux through the membranes monotonically increases with increasing temperatures, which is ascribed to the faster oxygen surface exchange rate and improved diffusion of bulk oxygen ions induced by higher temperatures [40]. In addition, the oxygen permeation flux slightly decreases with increasing amounts of doped Zr. The result is attributed to a lower concentration of oxygen vacancy concentration and a stronger average binding energy of metal–oxygen, which makes the transport of oxygen ions through the membranes more difficult [28]. An oxygen permeation flux of 0.35 ml min^{-1} cm^{-2} is achieved for the SDC–BLF membrane at 925 °C, which is significantly lower than a value of 1.96 ml min^{-1} cm^{-2} reported by Kida on single-phase $Ba_{0.95}La_{0.05}FeO_{3-\delta}$ at 930 °C [21]. This is mainly because the SDC phase is non-conducting to electrons; thus, it impedes the transport of electrons through the membrane [17]. Since the substitution of zirconium is not favorable for oxygen permeability, it is necessary to investigate the ideal zirconium content for the Zr-doped CO_2-resistant SDC–BLFZ membranes.

It is well known that oxygen permeation through an MIEC membrane is controlled by the diffusion rate of oxygen ions through the membrane and/or the surface oxygen exchange rate on the gas–membrane interface [39,41]. To investigate the rate-limiting step of the SDC–BLFZ membranes, the sample exhibiting the best oxygen permeability under He ($x = 0$) was chosen to study the thickness dependence of oxygen permeability, as shown in Fig. 6(b). From Fig. 6(b), it is clear that oxygen permeation flux significantly increases with decreasing thickness in the whole range

of testing temperatures. Evidently, membrane thickness significantly impacts the oxygen permeation flux of the SDC–BLFZ membranes. Therefore, the oxygen permeability of these membranes can be significantly improved by reducing their thickness. The highest oxygen permeation flux for a 0.6 mm thick SDC–BLF membrane reaches 0.54 ml min^{-1} cm^{-2} at 925 °C, which is comparable to that exhibited by most dual-phase membranes listed in Table 1.

For a fluorite-perovskite dual-phase membrane, its oxygen permeability is usually determined by the transport of oxygen ions through the membrane because electrons transport much faster than that of oxygen ions [26]. Since oxygen ions transport mainly through IC phase, on the premise that the two phases have respectively formed an interpenetrating continuous network, the increment of IC phase should increase its oxygen permeability. To optimize the ratio between SDC phase and BLFZ phase and investigate the influence of SDC content on the CO_2-tolerance of SDC-BLFZ, oxygen permeation flux through *x* wt% SDC-(1-*x*) wt% $BLFZ_{0.10}$ (*x* = 50-70) were carried out using He and CO_2 as sweep gas. As shown in Fig. 7, when He is used as sweep gas, 60 wt% SDC-40 wt% $BLFZ_{0.10}$ yields the highest oxygen permeation flux whereas 70 wt% SDC-30 wt% $BLFZ_{0.10}$ has the lowest one, which is similar to literature [42,43]. For the latter, although it has the largest ratio of SDC, $BLFZ_{0.10}$ could probably fail to form a continuous network, thus 70 wt% SDC-30 wt% $BLFZ_{0.10}$ shows the worst permeability. When the sweep gas is switched to CO_2/He mixture gas or pure CO_2, oxygen permeation flux of SDC-$BLFZ_{0.10}$ upon exposure to CO_2 drops less remarkably as the ratio of SDC increases. For example, oxygen permeation flux through 50 wt% SDC-50 wt% $BLFZ_{0.10}$ is higher than that of 70 wt% SDC-30 wt% $BLFZ_{0.10}$ when He is used as sweep gas; however, when the sweep gas is switched to 50%CO_2/He or CO_2, oxygen

permeability of the latter one is higher than that of the former one. Evidently, the addition of SDC can significantly enhance the CO_2-stability of SDC-BLFZ.

Fig. 8(a) shows the effects of CO_2 concentration in the sweep gas on the oxygen permeation flux through the SDC–BLFZ membranes with different Zr contents as a function of time at 925 °C. From the figure, all membranes exhibit a stable oxygen permeation flux in the whole testing process when pure He is used as the sweep gas. Some researchers have reported that the reaction between the two phases could lead to the performance degradation of dual-phase composites [44,45]. However, no performance degradation is observed in our experiment, suggesting excellent chemical compatibility between SDC and BLF. The oxygen permeation flux of all samples decreases upon exposure to a gas mixture of 15 vol% CO_2 and He. CO_2 exerts the following effects on the oxygen permeation flux of membranes: 1. It reacts with alkaline metals and forms carbonates on the membrane surface, and 2. It adsorbs on the membrane surface and subsequently influences surface oxygen exchange [7,40,46]. In this case, since most of the A-sites of the EC phase (BLF) are occupied by Ba^{2+}, it is assumed that both aspects are attributed to permeability degradation. After switching the sweep gas to a gas mixture of 50 vol% CO_2 and He and pure CO_2, the oxygen permeation flux of samples with $x = 0$ and $x = 0.05$ starts to decrease with time, whereas the remaining samples still maintain a stable flux without an apparent decrement, indicating that Zr doping successfully enhances the CO_2 resistance of the SDC–BLFZ membranes [5,14]. Upon exposure to He again, the oxygen permeation flux of all samples recovers its initial value with He as the sweep gas in the first stage, which is attributed to the good structural reversibility of the samples under low oxygen partial pressure and CO_2-containing atmospheres.

Fig. 8(b) shows the XRD patterns of the permeating side of all membranes after

the oxygen permeability with different concentrations of CO_2 as the sweep gas. As mentioned above, some researchers have reported that the two phases of a dual-phase oxide react with each other and form secondary phases on the boundary [44,47,48]. Besides, some composites could partly decompose and form foreign phases under operating conditions [49]. Fortunately, no apparent secondary phase generated from the reaction between SDC and BLF or from the decomposition of BLF is detected after the experiments, indicating good compatibility between the two phases and favorable structure stability of BLF during oxygen permeation using a gas mixture of CO_2 and He. The peak intensity of BLF is relatively weakened after the experiments, which is possibly because the initial crystal ordering deteriorates during oxygen permeation.

To evaluate the possible application of the SDC–BLFZ membranes in oxy-fuel combustion technology and further investigate the influence of Zr doping on the CO_2 tolerance of SDC–BLFZ, long-term oxygen permeation flux with pure CO_2 as the sweep gas is also performed on samples with x = 0 and 0.15 at 925 °C, as shown in Fig. 9(a). The samples were first swept by He for approximately 17 h, followed by pure CO_2 for more than 80 h. As shown in the figure, the oxygen permeation flux rapidly decreases at first and then approximately levels off for samples with x = 0 (thickness: 0.6 mm and 1.0 mm) with CO_2 as the sweep gas, whereas it remains almost unchanged for sample with x = 0.15. After exposure to pure CO_2 for ca. 60 h, samples with x = 0 and thickness of 0.6 mm and 1.0 mm exhibited oxygen permeation flux of approximately 0.34 ml min^{-1} cm^{-2} and 0.22 ml min^{-1} cm^{-2}, respectively. Compared with the oxygen permeation flux under air/He gradient, a decrease of 38% is observed for both thickness values. The reaction degree between SDC–BLF and CO_2 and the amount of carbonates formed on the membrane surface is presumably the

same for both thickness values, i.e., independent of membrane thickness. The oxygen permeation flux for $x = 0.15$ negligibly decreases and levels off at 0.24 ml min^{-1} cm^{-2} even after exposure to CO_2 for more than 80 h, which is only 19% lower than that under an air/He gradient. This value is comparable to most dual-phase and some CO_2-tolerant single-phase composites listed in Table 1 (references therein). Since the oxygen permeation flux of these membranes can be further increased by reducing their thickness, they have significant potential in the application of oxy-fuel combustion technology.

Fig. 9(b) shows the XRD patterns of membranes after long-term experiment. For $x = 0$, reflection peaks indexed as $BaCO_3$, which are generated from the reaction between CO_2 and Ba^{2+}, are detected on the sweep side. However, for the sample with $x = 0.15$, no carbonates are observed on the sweep side even after exposure to pure CO_2 for over 80 h, indicating excellent stability against CO_2. This result is in agreement with TG-DSC experiments. Besides, no other impurity phases were observed on both sides of the membrane. Evidently, 15% of the Zr substituted for Fe significantly or even totally restrains the reaction between BLFZ and CO_2 and successfully enhances the stability of the membrane under large oxygen partial pressure gradient and CO_2-containing atmospheres.

Fig. 10 shows the surface SEM micrographs of the fresh sintered and the spent membranes of samples with $x = 0$ and 0.15. The surface SEM images of the sintered membranes of samples with $x = 0$ and 0.15 are shown in Fig. 10(a) and (b), respectively. Energy-dispersive X-ray spectroscopy (EDS) analysis shows that the larger grains with a size range between 300 and 1000 nm mainly contain Ce and Sm, which are assignable to SDC. In contrast, the smaller grains with a size of 20–300 nm are attributed to perovskite BLFZ, while the black spots are pinholes. As shown in the

figure, the sample with $x = 0$ has relatively larger perovskite particles as compared to those of the sample with $x = 0.15$, possibly because larger Zr ions are unfavorable for the calcination of BLFZ. Fig. 10(c) shows the micrographs of the cross-section of the fresh membrane with $x = 0$. It can be seen that the membrane is very dense. Except for some small closed pinholes, no connected pores are observed. Besides, gas-tightness of all membranes has been ensured by monitoring nitrogen content in the permeated gas before oxygen permeation flux experiments. Fig. 10(d) shows the secondary electron (left) and backscattered electron (right) micrographs of the cross-section of the fresh membrane with $x = 0.15$ at the same position. The backscattered electron micrograph of the membrane in Fig. 10(d) (right) shows three different contrast levels (light, gray and dark). Since the contribution of the back-scattered electrons to the SEM signal intensity is proportional to the atomic number and the average atomic number of SDC is larger than that of $BLFZ_{0.15}$, one can conclude that the light grains are SDC, while the gray ones are $BLFZ_{0.15}$ and the dark spots are pinholes. The uniform distribution of the light and gray grains gives firm evidence for the continuous network structure for both phases.

Fig. 10(e) and (f) shows the surface morphologies of the used membranes from the sweep side after the long-term experiment of samples with $x = 0$ and 0.15, respectively. As clearly shown, the membrane surface of the sample with $x = 0$ is badly corroded, and a part of the membrane surface is covered by several scale-like secondary phase particles. EDS analysis proves it to be the resultant $BaCO_3$, which is in accordance with XRD results. Numerous studies have reported that the oxygen permeation flux of single-phase perovskite composites with A-sites occupied by alkaline metals remarkably decreases upon exposure to CO_2 [10,11,16]. However, this phenomenon is not observed in our long-term experiment. Different from that of

single-phase composites, the surface of the dual-phase SDC–BLF membrane is majorly covered by CO_2-tolerant SDC; hence, $BaCO_3$ cannot grow into a continuous layer and cover the whole membrane surface even after exposure to CO_2 for over 80 h. That is why the oxygen permeation flux is partially reserved although most of the A-site lattices of perovskite BLF are occupied by Ba. However, for the sample with x = 0.15, apart from several white particles, which are determined to be $BaCO_3$, the rest of the membrane surface is nearly intact. Obviously, the substitution of 15% of Zr significantly lowers the basicity of BLF and suppresses the formation of $BaCO_3$.

4. Conclusions

Dual-phase membranes composed of SDC and Zr-doped perovskite BLF are successfully prepared by a combined EDTA–citrate complexing sol–gel method. Good chemical compatibility is observed between the two phases under sintering and different operating conditions. XPS results show that the basicity of BLFZ increases with increasing zirconium substitution, which is attributed to the higher O 1s binding energy induced by the stronger Zr–O bond strength as compared with that of Fe–O. A trace amount of doped zirconium slightly decreases the oxygen permeation flux of the SDC–BLFZ membranes but significantly enhances the stability of BLF under a low oxygen partial pressure and a large oxygen partial pressure gradient. After exposure to CO_2 for more than 80 h, a stable oxygen permeation flux of 0.24 and 0.22 ml min^{-1} cm^{-2} is achieved with 1 mm thickness for samples with x = 0.15 and 0, which are 19% and 38% lower than that with He as the sweep gas, respectively. Although most of the A-sites of the perovskite are occupied by barium, the reaction between BLF and CO_2 is largely restrained by the partial substitution of zirconium for iron. XRD and SEM results confirm that the reaction degree between CO_2 and samples with zirconium doping of 0.15 is rather weak, revealing SDC–BLFZ excellent CO_2 resistance and

possible application in oxy-fuel combustion technology.

Acknowledgments

This work was supported by the National Natural Science Foundation of China (No. 51474145), the National Science Fund for Distinguished Young Scholars (No. 51225401), the Shanghai Rising-Star Program (No. 15QA1402100) and Innovation Program of Shanghai Municipal Education Commission (No. 14YZ013).

References:

[1] R.S. Haszeldine, Carbon Capture and Storage: How Green Can Black Be?, Science 325 (2009) 1647−1652.

[2] D.M. D'Alessandro, B. Smit, J.R. Long, Carbon Dioxide Capture: Prospects for New Materials, Angew. Chem. Int. Ed. 49 (2010) 6058−6082.

[3] J. Davison, Performance and costs of power plants with capture and storage of CO_2, Energy 32 (2007) 1163−1176.

[4] E.S. Rubin, C. Chen, A.B. Rao, Cost and performance of fossil fuel power plants with CO_2 capture and storage, Energy Policy 35 (2007) 4444−4454.

[5] W. Chen, C.S. Chen, H.J.M. Bouwmeester, A. Nijmeijer, L. Winnubst, Oxygen-selective membranes integrated with oxy-fuel combustion, J. Membr. Sci. 463 (2014) 166−172.

[6] A. Leo, S.M. Liu, J.C.D. da Costa, Development of mixed conducting membranes for clean coal energy delivery, Int. J. Greenhouse Gas Control 3 (2009) 357−367.

[7] X.F. Zhu, H.Y. Liu, Y. Cong, W.S. Yang, Novel dual-phase membranes for CO_2 capture via an oxyfuel route, Chem. Commun. 48 (2012) 251−253.

[8] Y. Teraoka, H.M. Zhang, S. Furukawa, N. Yamazoe, Oxygen permeation through perovskite-type oxides, Chem. Lett. 14 (1985) 1743−1746.

[9] Z.P. Shao, W.S. Yang, Y. Cong, H. Dong, J.H. Tong, G.X. Xiong, Investigation of the permeation behavior and stability of a $Ba_{0.5}Sr_{0.5}Co_{0.8}Fe_{0.2}O_{3-\delta}$ oxygen membrane, J. Membr. Sci. 172 (2000) 177−188.

[10] J.X. Yi, M. Schroeder, T. Weirich, J. Mayer, Behavior of Ba(Co, Fe, Nb)$O_{3-\delta}$ Perovskite in CO_2-Containing Atmospheres: Degradation Mechanism and Materials Design, Chem. Mater. 22 (2010) 6246−6253.

[11] O. Czuprat, M. Arnold, S. Schirrmeister, T. Schiestel, J. Caro, Influence of CO_2 on the oxygen permeation performance of perovskite-type $BaCo_xFe_yZr_zO_{3-\delta}$ hollow fiber membranes, J. Membr. Sci. 364 (2010) 132−137.

[12] T. Klande, O. Ravkina, A. Feldhoff, Effect of A-site lanthanum doping on the CO_2 tolerance of $SrCo_{0.8}Fe_{0.2}O_{3-\delta}$ oxygen-transporting membranes, J. Membr. Sci. 437 (2013) 122−130.

[13] X.L. Dong, G.R. Zhang, Z.K. Liu, Z.X. Zhong, W.Q. Jin, N.P. Xu, CO_2-tolerant mixed conducting oxide for catalytic membrane reactor, J. Membr. Sci. 340 (2009) 141−147.

[14] J.X. Yi, M. Schroeder, M. Martin, CO_2-Tolerant and Cobalt-Free $SrFe_{0.8}Nb_{0.2}O_{3-\delta}$ Perovskite Membrane for Oxygen Separation, Chem. Mater. 25 (2013) 815−817.

[15] W. Chen, C.S. Chen, L. Winnubst, Ta-doped $SrCo_{0.8}Fe_{0.2}O_{3-\delta}$ membranes: Phase stability and oxygen permeation in CO_2 atmosphere, Solid State Ionics 196 (2011) 30−33.

[16] M. Arnold, H.H. Wang, A. Feldhoff, Influence of CO_2 on the oxygen permeation performance and the microstructure of perovskite-type $(Ba_{0.5}Sr_{0.5})(Co_{0.8}Fe_{0.2})O_{3-\delta}$ membranes, J. Membr. Sci. 293 (2007) 44−52.

[17] J. Xue, Q. Liao, Y.Y. Wei, Z. Li, H. Wang, A CO_2-tolerance oxygen permeable $60Ce_{0.9}Gd_{0.1}O_{2-\delta}$−$40Ba_{0.5}Sr_{0.5}Co_{0.8}Fe_{0.2}O_{3-\delta}$ dual phase membrane, J. Membr. Sci. 443 (2013) 124−130.

[18] T. Nagai, W. Ito, T. Sakon, Relationship between cation substitution and stability of perovskite structure in $SrCoO_{3-\delta}$-based mixed conductors, Solid State Ionics 177 (2007) 3433−3444.

[19] Z.P. Shao, G.X. Xiong, J.H. Tong, H. Dong, W.S. Yang, Ba effect in doped $Sr(Co_{0.8}Fe_{0.2})O_{3-\delta}$ on the phase structure and oxygen permeation properties of the dense ceramic membranes, Sep. Purif. Technol. 25 (2001) 419−429.

[20] C.Y. Park, T.H. Lee, S.E. Dorris, U. Balachandran, A cobalt-free oxygen transport membrane, $BaFe_{0.9}Zr_{0.1}O_{3-\delta}$, and its application for producing hydrogen, Int. J. Hydrogen Energy 38 (2013) 6450−6459.

[21] T. Kida, D. Takauchi, K. Watanabe, M. Yuasa, K. Shimanoe, Y. Teraoka, N. Yamazoe, Oxygen Permeation Properties of Partially A-Site Substituted $BaFeO_{3-\delta}$ Perovskites, J. Electrochem. Soc. 156 (2009) E187−E191.

[22] D.J. Chen, C. Chen, F.F. Dong, Z.P. Shao, F. Ciucci, Cobalt-free polycrystalline $Ba_{0.95}La_{0.05}FeO_{3-\delta}$ thin films as cathodes for intermediate-temperature solid oxide fuel cells, J. Power Sources 250 (2014) 188−195.

[23] B. Jiang, H.W. Cheng, L.F. Luo, X.G. Lu, Z.F. Zhou, Oxygen Permeation and Stability of $Ce_{0.8}Gd_{0.2}O_{2-\delta}$−$PrBaCo_{2-x}Fe_xO_{5+\delta}$ Dual−phase Composite Membranes, J. Mater. Sci. Technol. 30 (2014) 1174−1180.

[24] H.W. Cheng, X.G. Lu, D.H. Hu, Y.W. Zhang, W.Z. Ding, H.L. Zhao, Hydrogen production by catalytic partial oxidation of coke oven gas in $BaCo_{0.7}Fe_{0.2}Nb_{0.1}O_{3-\delta}$ membranes with surface modification, Int. J. Hydrogen Energy, 36 (2011) 528−538.

[25] Y. Li, H.L. Zhao, N.S. Xu, Y.N. Shen, X.G. Lu, W.Z. Ding, F.S. Li, Systematic investigation on structure stability and oxygen permeability of Sr-doped $BaCo_{0.7}Fe_{0.2}Nb_{0.1}O_{3-\delta}$ ceramic membranes, J. Membr. Sci. 362 (2010) 460−470.

[26] T. Chen, H.L. Zhao, Z.X. Xie, J. Wang, Y. Lu, N.S. Xu, $Ce_{0.8}Sm_{0.2}O_{2-\delta}$−$PrBaCo_2O_{5+\delta}$ dual-phase membrane: Novel preparation and improved oxygen permeability, J. Power Sources 223 (2013) 289−292.

[27] F.F. Dong, D.J. Chen, Y.B. Chen, Q. Zhao, Z.P. Shao, La-doped $BaFeO_{3-\delta}$ perovskite as a cobalt-free oxygen reduction electrode for solid oxide fuel cells with oxygen-ion conducting electrolyte, J. Mater. Chem. 22 (2012) 15071−15079.

[28] O. Ravkina, T. Klande, A. Feldhoff, Investigation of Zr-doped BSCF perovskite membrane for oxygen separation in the intermediate temperature range, J. Solid State Chem. 201 (2013) 101−106.

[29] H.W. Cheng,W.L. Yao, X.G. Lu, Z.F. Zhou, C.H. Li, J.Z. Liu, Structural stability and oxygen permeability of $BaCo_{0.7}Fe_{0.2}M_{0.1}O_{3-\delta}$ (M = Ta, Nb, Zr) ceramic

membranes for producing hydrogen from coke oven gas, Fuel Process. Technol. 131 (2015) 36−44.

[30] G.R. Zhang, Z.K. Liu, N. Zhu, W. Jiang, X.L. Dong, W.Q. Jin, A novel Nb_2O_5-doped $SrCo_{0.8}Fe_{0.2}O_{3-\delta}$ oxide with high permeability and stability for oxygen separation, J. Membr. Sci. 405−406 (2012) 300−309.

[31] X.T. Liu, H.L. Zhao, J.Y. Yang, Y. Li, T. Chen, X.G. Lu, W.Z. Ding, F.S. Li, Lattice characteristics, structure stability and oxygen permeability of $BaFe_{1-x}Y_xO_{3-\delta}$ ceramic membranes, J. Membr. Sci. 383 (2011) 235−240.

[32] M. Ghaffaria, M. Shannon, H. Hui, O.K. Tan, A. Irannejad, Preparation, surface state and band structure studies of $SrTi_{(1-x)}Fe_{(x)}O_{(3-\delta)}$ (x = 0−1) perovskite-type nano structure by X-ray and ultraviolet photoelectron spectroscopy, Surf. Sci. 606 (2012) 670−677.

[33] C. Chen, D.J. Chen,Y. Gao, Z.P. Shao, F. Ciucci, Computational and experimental analysis of $Ba_{0.95}La_{0.05}FeO_{3-\delta}$ as a cathode material for solid oxide fuel cells, J. Mater. Chem. A 2 (2014) 14154−14163.

[34] Z.H. Du, H.L. Zhao, Y.N. Shen, L. Wang, M.Y. Fang, K. Świerczek, K. Zheng, Evaluation of $La_{0.3}Sr_{0.7}Ti_{1-x}Co_xO_3$ as a potential cathode material for solid oxide fuel cells, J. Mater. Chem. A 2 (2014) 10290−10299.

[35] Q. Zeng, Y. Zuo, C. Fan, C. Chen, CO_2-tolerant oxygen separation membranes targeting CO_2 capture application, J. Membr. Sci. 335 (2009) 140−144.

[36] H.J.M. Bosman, A.P. Pijpers, A.W.M.A. Jaspers, An X-Ray Photoelectron Spectroscopy Study of the Acidity of SiO_2−ZrO_2 Mixed Oxides, J. Catal. 161 (1996) 551−559.

[37] Q. Zhen, Q. Yun, H.J. Wang, C. Ding, W.Z. Ding, X.G. Lu, Investigation of chemical stability and oxygen permeability of perovskite-type $Ba_{0.5}Sr_{0.5}Co_{0.8}Fe_{0.2}O_{3-\delta}$ and $BaCo_{0.7}Fe_{0.2}Nb_{0.1}O_{3-\delta}$ ceramic membranes, Solid State Ionics 189 (2011) 50−55.

[38] J.Z. Liu, H.W. Cheng, B. Jiang, X.G. Lu, W.Z. Ding, Effects of tantalum content on the structure stability and oxygen permeability of $BaCo_{0.7}Fe_{0.3-x}Ta_xO_{3-\delta}$ ceramic membrane, Int. J. Hydrogen Energy 38 (2013) 11090−11096.

[39] B. Jiang, H.W. Cheng, L.F. Luo, X.G. Lu, N.J. Zhang, J.Z. Liu, Oxygen permeation and phase structure properties of partially A-site substituted $BaCo_{0.7}Fe_{0.225}Ta_{0.075}O_{3-\delta}$ perovskites, J. Energ. Chem. 23 (2014) 164−170.

[40] Y.Y. Wei, J. Tang, L.Y. Zhou, J. Xue, Z. Li, H.H. Wang, Oxygen Separation through U-Shaped Hollow Fiber Membrane Using Pure CO_2 as Sweep Gas, AIChE J. 58 (2012) 2856−2864.

[41] T. Chen, H.L. Zhao, N.S. Xu, Y. Li, X.G. Lu, W.Z. Ding, F.S. Li, Synthesis and oxygen permeation properties of a $Ce_{0.8}Sm_{0.2}O_{2-\delta}$−$LaBaCo_2O_{5+\delta}$ dual-phase composite membrane, J. Membr. Sci. 370 (2011) 158−165.

[42] H.X. Luo, H.Q. Jiang, K. Efimov, F.Y. Liang, H.H. Wang, J. Caro, CO_2-Tolerant Oxygen-Permeable Fe_2O_3-$Ce_{0.9}Gd_{0.1}O_{2-\delta}$ Dual Phase Membranes, Ind. Eng. Chem. Res. 50 (2011) 13508–13517.

[43] L.F. Luo, H.W. Cheng, G.S. Li, X.G. Lu, B. Jiang, Oxygen permeability and CO_2-tolerance of $Ce_{0.8}Gd_{0.2}O_{2-\delta}$-$LnBaCo_2O_{5+\delta}$ dual-phase membranes, J. Energ. Chem. 24 (2015) 15−22.

[44] V.V. Kharton, A.V. Kovalevsky, A.P. Viskup, F.M. Figueiredo, A.A. Yaremchenko, E.N. Naumovich, F.M.B. Marques, Oxygen permeability and Faradaic efficiency of $Ce_{0.8}Gd_{0.2}O_{2-\delta}$−$La_{0.7}Sr_{0.3}MnO_{3-\delta}$ composites, J. Eur. Ceram. Soc. 21 (2001) 1763−1767.

[45] W. Li, T.F. Tian, F.Y. Shi, Y.S. Wang, C.S. Chen, $Ce_{0.8}Sm_{0.2}O_{2-\delta}$−$La_{0.8}Sr_{0.2}MnO_{3-\delta}$ Dual-Phase Composite Hollow Fiber Membrane for Oxygen Separation, Ind. Eng. Chem. Res. 48 (2009) 5789−5793.

[46] X.F. Zhu, Y. Liu, Y. Cong, W.S. Yang, $Ce_{0.85}Sm_{0.15}O_{1.925}$−$Sm_{0.6}Sr_{0.4}Al_{0.3}Fe_{0.7}O_3$ dual-phase membranes: One-pot synthesis and stability in a CO_2 atmosphere, Solid State Ionics 253 (2013) 57−63.

[47] A.L. Shaula, V.V. Kharton, F.M.B. Marques, Phase interaction and oxygen transport in $La_{0.8}Sr_{0.2}Fe_{0.8}Co_{0.2}O_3$−$(La_{0.9}Sr_{0.1})_{0.98}Ga_{0.8}Mg_{0.2}O_3$ composites J. Eur. Ceram. Soc. 24 (2004) 2631−2639.

[48] U. Nigge, H.-D. Wiemhöfer, E.W.J. Römer, H.J.M. Bouwmeester, T.R. Schulte, Composites of $Ce_{0.8}Gd_{0.2}O_{1.9}$ and $Gd_{0.7}Ca_{0.3}CoO_{3-\delta}$ as oxygen permeable membranes for exhaust gas sensors, Solid State Ionics 146 (2002) 163–174.

[49] T. Chen, H.L. Zhao, Z.X. Xie, L.C. Feng, X.G. Lu, W.Z. Ding, F.S. Li, Electrical conductivity and oxygen permeability of $Ce_{0.8}Sm_{0.2}O_{2-\delta}$–$PrBaCo_2O_{5+\delta}$ dual-phase composites, Int. J. Hydrogen Energy 37 (2012) 5277–5285.

[50] H.X. Luo, K. Efimov, H.Q. Jiang, A. Feldhoff, H.H. Wang, J. Caro, CO_2-Stable and Cobalt-Free Dual-Phase Membrane for Oxygen Separation, Angew. Chem. Int. Ed. 50 (2011) 759–763.

Table 1 Oxygen permeation flux of some reported oxygen-permeable composites with the CO_2/He as sweep gas.

Composition	Thickness (mm)	Temperature (°C)	JO_2 air/helium ml min^{-1} cm^{-2}	JO_2 air/CO_2 ml min^{-1} cm^{-2}	JO_2 decrease	Ref.
$BaCo_xFe_yZr_zO_{3-\delta}$	0.14	900	3.1	0.4[a]	87%	11
$La_{0.85}Ce_{0.1}Ga_{0.3}Fe_{0.65}Al_{0.05}O_{3-\delta}$	1.0	950	0.26	0.17[b]	35%	13
$Ba_{0.5}Sr_{0.5}Co_{0.8}Fe_{0.2}O_{3-\delta}$	1.0	875	1.9	0	100%	16
$60Ce_{0.9}Gd_{0.1}O_{2-\delta}$–$40Ba_{0.5}Sr_{0.5}Co_{0.8}Fe_{0.2}O_{3-\delta}$	0.5	950	1.79	0.67	63%	17
$60Ce_{0.9}Gd_{0.1}O_{2-\delta}$–$40Fe_2O_3$	0.5	1000	0.18	0.16	11%	42
$60Ce_{0.9}Gd_{0.1}O_{2-\delta}$–$40NiFe_2O_4$	0.5	1000	0.31	0.27	13%	50
SDC–BLF	0.6	925	0.54	0.34	38%	This study
SDC–$BLF_{0.85}Z_{0.15}$	1.0	925	0.30	0.24	19%	This study

[a] Sweep gas: 10% CO_2/90% He
[b] Sweep gas: 20% CO_2/80% He

Fig. 1 XRD patterns of (a) SDC and BLFZ powders calcined at 650 °C and 850 °C for 5 h, respectively; (b) SDC–BLFZ membranes sintered at 1200 °C for 5 h.

Fig. 2 O_2–TPD profiles of BLFZ.

Fig. 3 XPS spectra of Fe 2p of (a) BLF and (b) $BLF_{0.90}Z_{0.10}$.

Fig. 4 XPS spectra of O 1s of (a) BLF and (b) $BLF_{0.90}Z_{0.10}$.

Fig. 5 (a) TG–DSC curves of SDC–BLFZ under 50 vol% CO_2/N_2; (b) TG curves of SDC–BLF and SDC–$BLF_{0.85}Z_{0.15}$ under 50 vol% CO_2/N_2.

Fig. 6 Temperature dependence of oxygen permeation flux through (a) SDC–BLFZ membranes with 1.0 mm thickness and (b) SDC–BLF membranes with different thickness at 925 °C under air/He gradient. Conditions: He, 100 ml min^{-1}; air, 300 ml min^{-1}.

Fig. 7 Time dependence of oxygen permeation flux through 1.0 mm thick *x* wt% SDC-(1-*x*) wt% $BLFZ_{0.10}$ (*x* = 50-70) membranes as a function of CO_2 concentrations at 925 °C.

Fig. 8 (a) Time dependence of oxygen permeation flux through 1.0 mm thick SDC–BLFZ membranes as a function of CO_2 concentrations at 925 °C and (b) XRD patterns of the permeation side of the spent membranes.

Fig. 9 (a) Long-term oxygen permeation tests of SDC–BLF and SDC–$BLF_{0.85}Z_{0.15}$ membranes at 925 °C with He or CO_2 as the sweep gas and (b) XRD patterns of the spent membranes.

Fig. 10 SEM micrographs of fresh and spent membranes. The surface of the fresh (a) SDC–BLF and (b) SDC–$BLF_{0.85}Z_{0.15}$. The cross-section of fresh (c) SDC–BLF

and (d) SDC–$BLF_{0.85}Z_{0.15}$ in secondary electron (left) and backscattered electron (right) mode, respectively. The permeation side of the spent (e) SDC–BLF and (f) SDC–$BLF_{0.85}Z_{0.15}$ in the long-term experiment. The inset in (f) shows a magnified image of the microstructure.

Highlights:

1. $Ce_{0.8}Sm_{0.2}O_{2-\delta}$–$Ba_{0.95}La_{0.05}Fe_{1-x}Zr_xO_{3-\delta}$ membranes were successful synthesized.
2. The highest oxygen permeation flux of 0.54 ml min^{-1} cm^{-2} was achieved.
3. The oxygen permeability under air/CO_2 is only 19% lower than that of air/He.
4. Effects of Zr–doping on the performances of membranes were studied in detail.

Figure 1

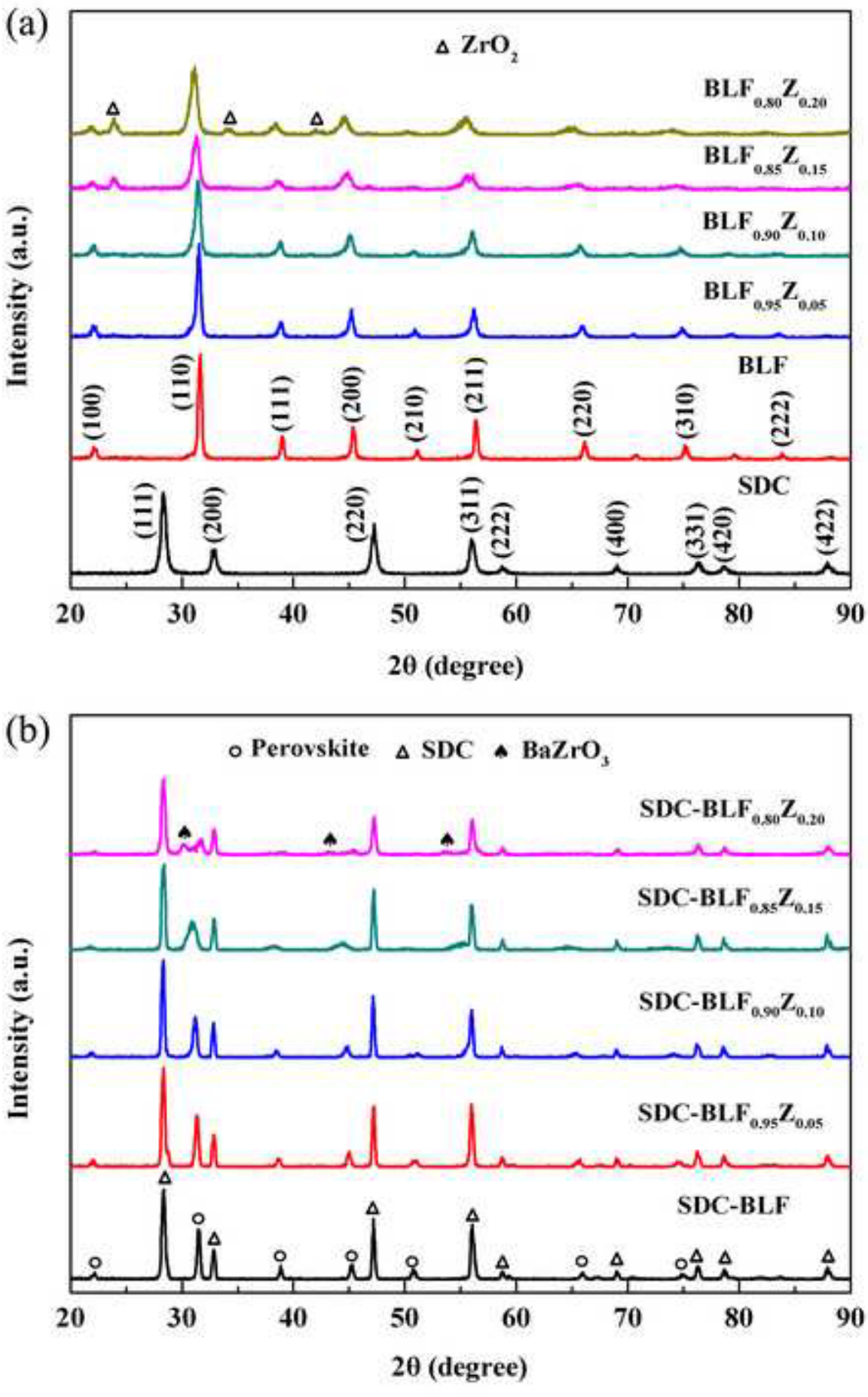

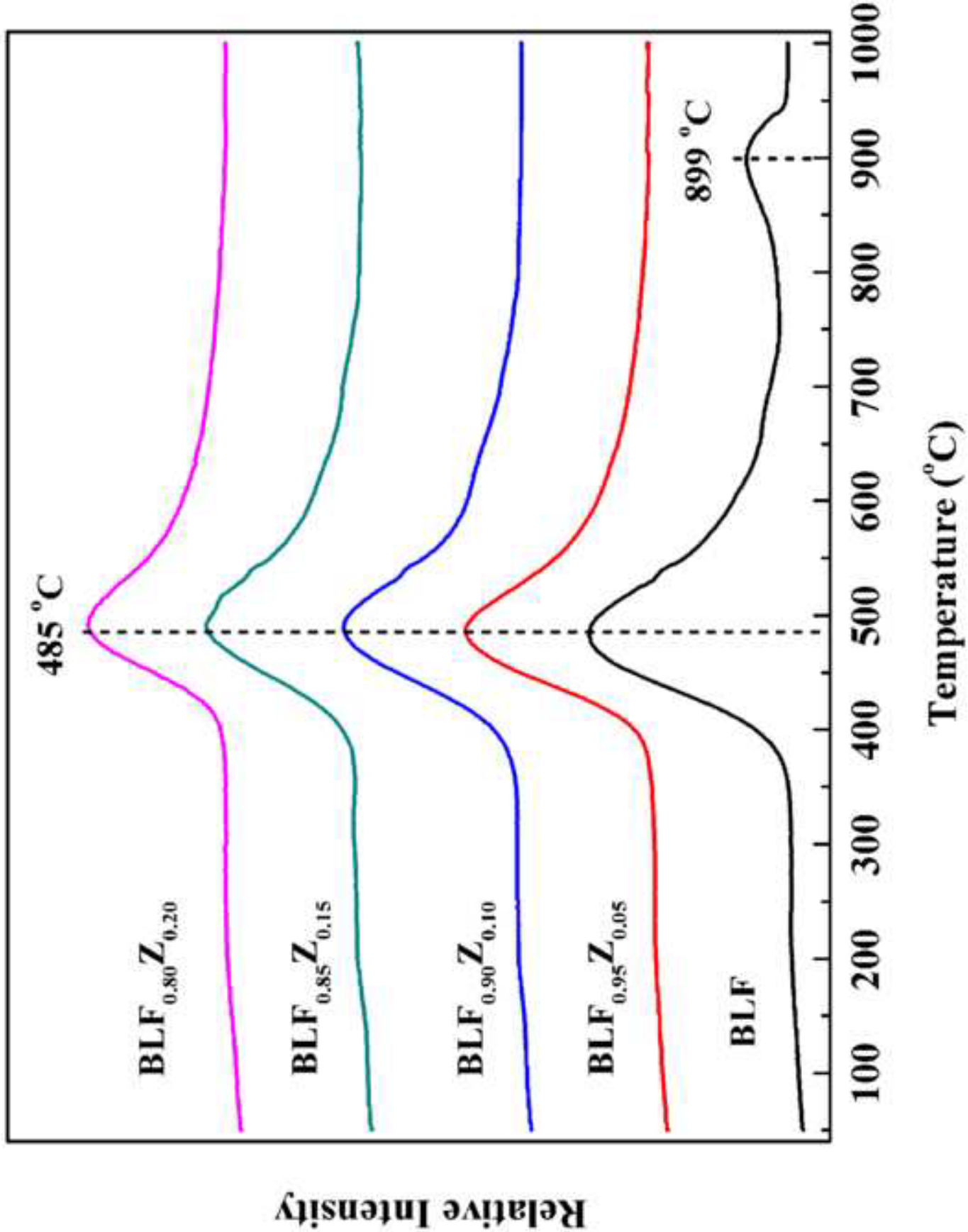

Figure 2

Figure 3

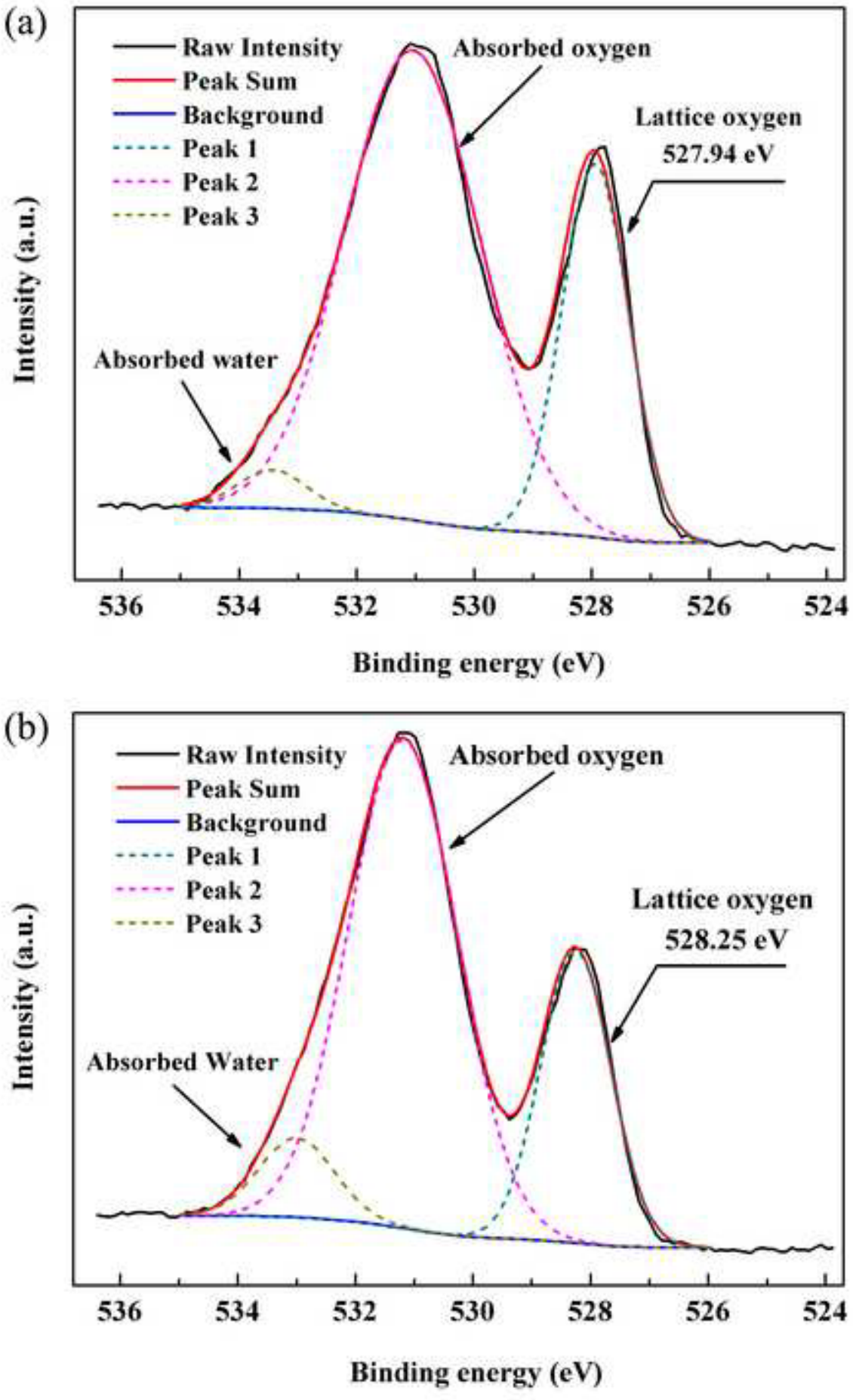

Figure 4

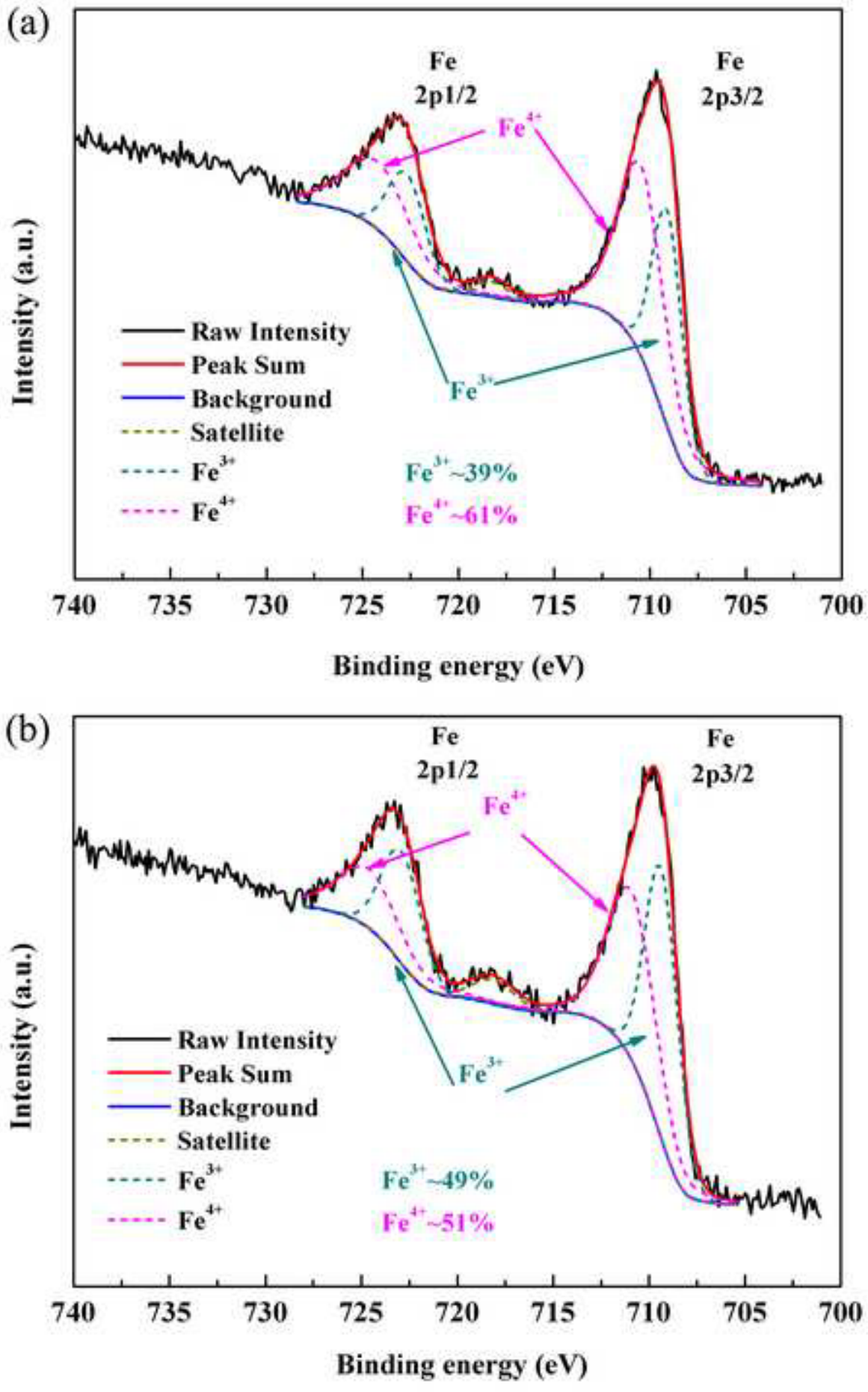

Figure 5

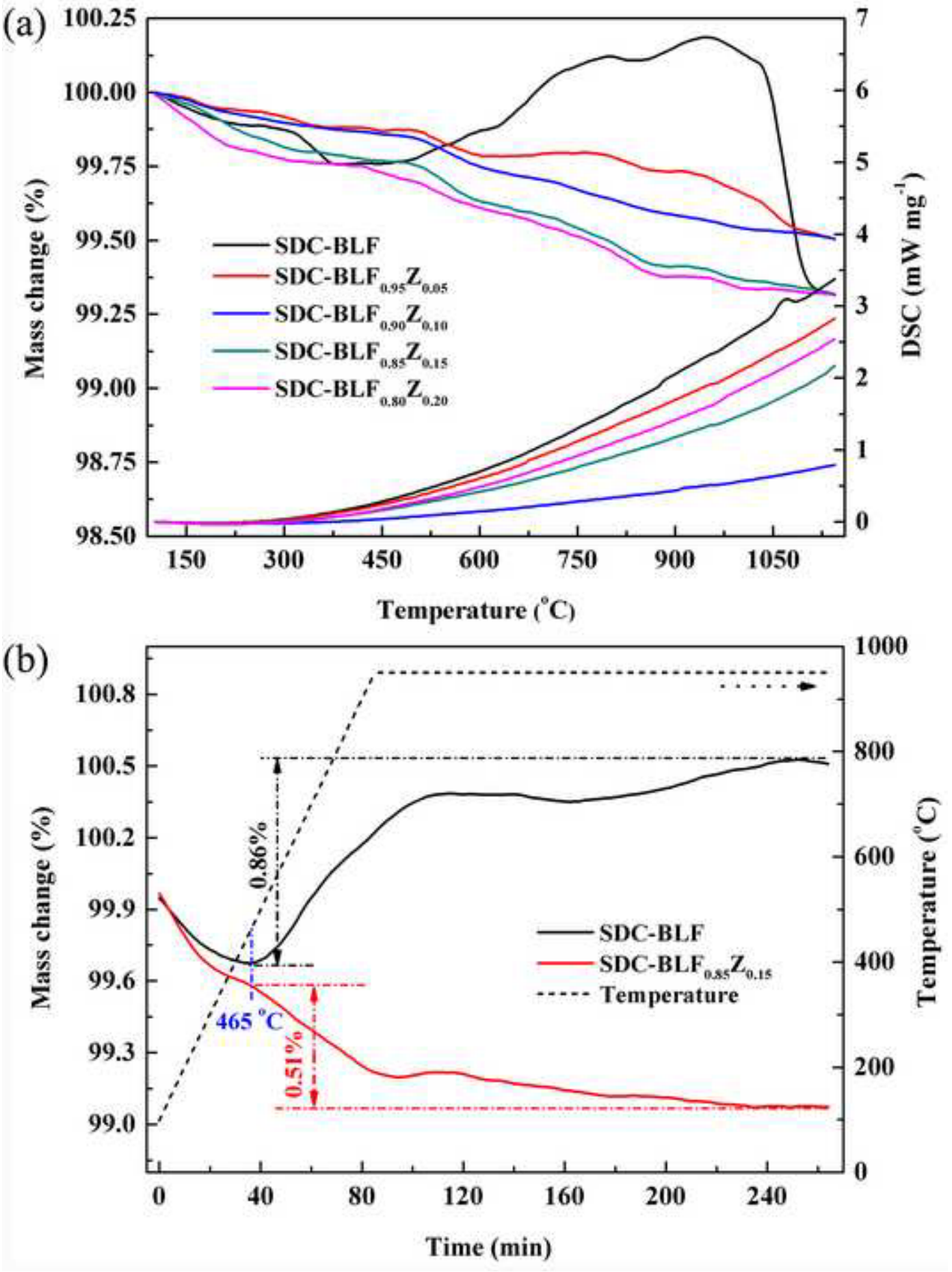

Figure 6

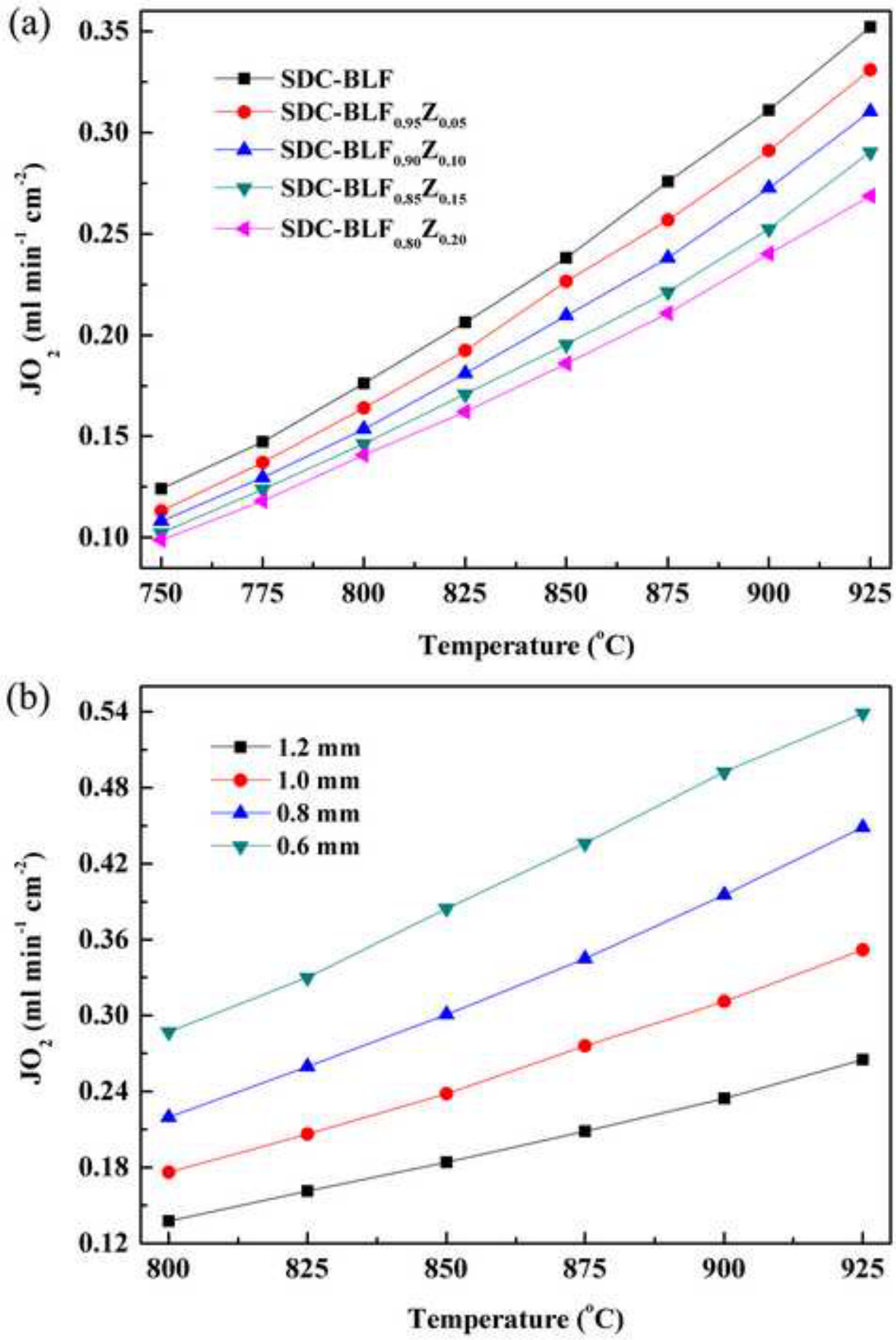

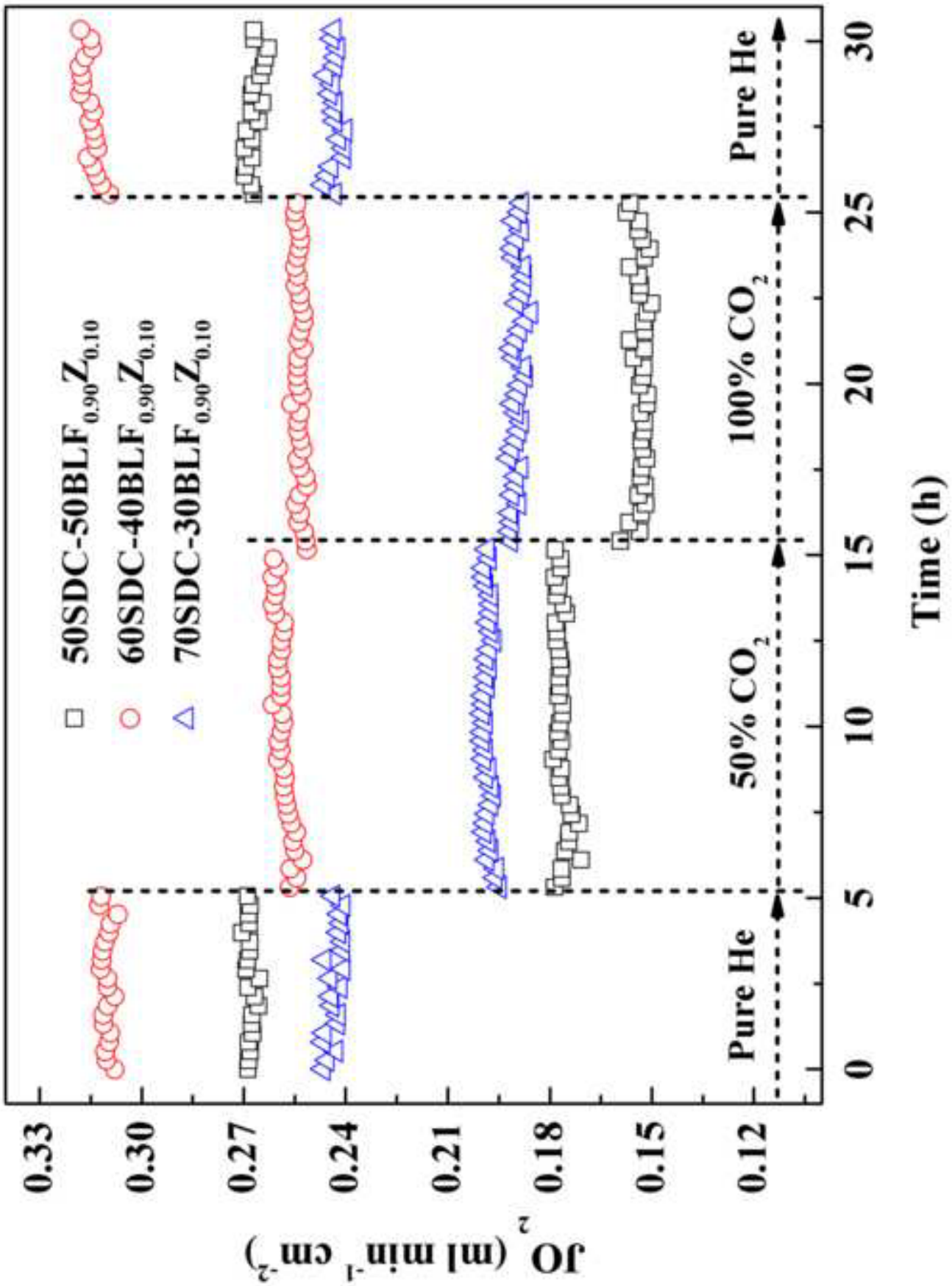
50SDC-50BLF0.90Z0.10
60SDC-40BLF0.90Z0.10
70SDC-30BLF0.90Z0.10
Pure He
50% CO2
100% CO2
Pure He
Time (h)
jO2 (ml min-1 cm-2)
0.33
0.30
0.27
0.24
0.21
0.18
0.15
0.12
0
5
10
15
20
25
30

Figure-7

Figure-8

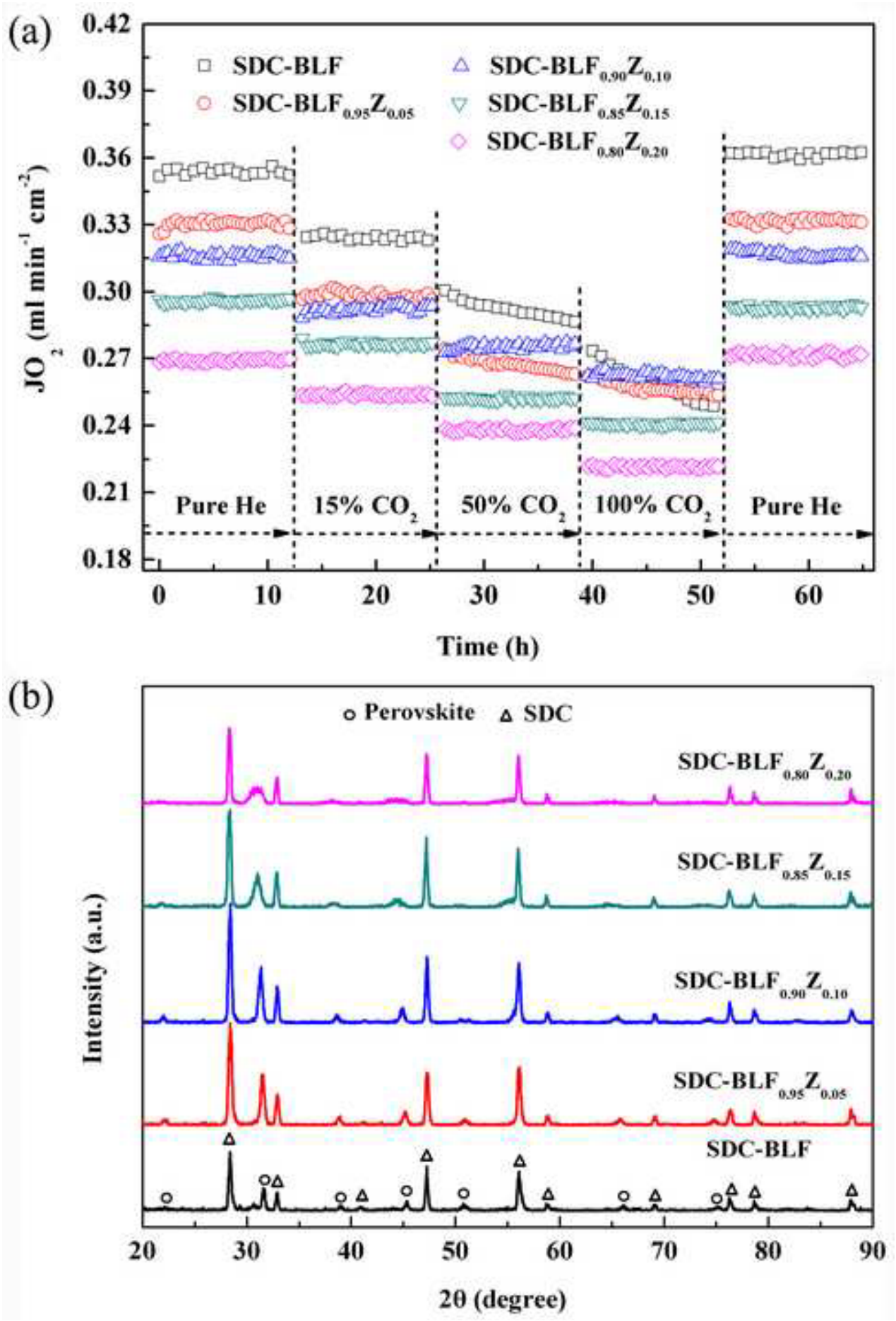

Figure-9

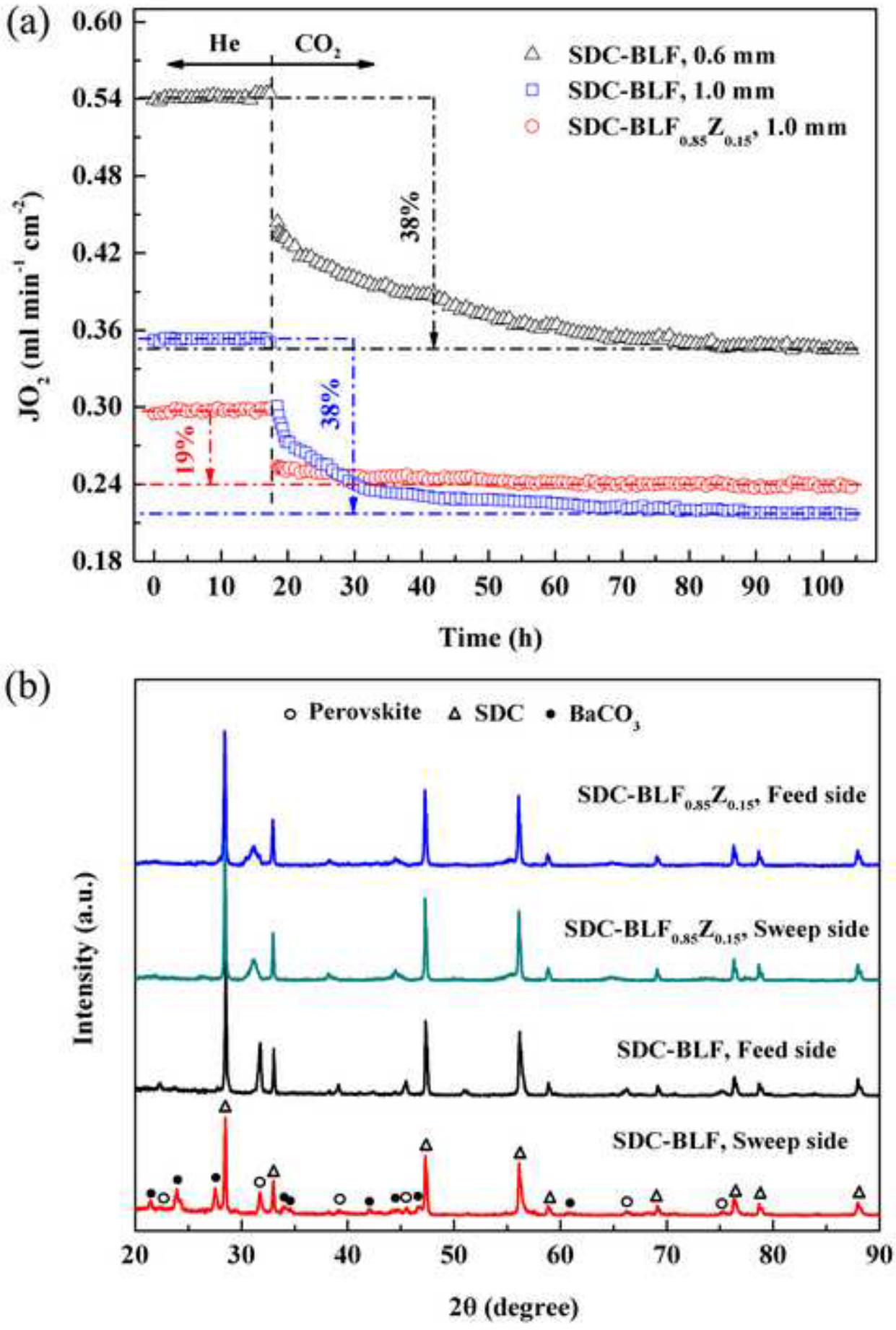

Figure-10